Chinese Chemical Letters 31 (2020) 988–991

Contents lists available at ScienceDirect

Chinese Chemical Letters

journal homepage: www.elsevier.com/locate/cclet

Communication

Pt immobilized spontaneously on porous MXene/MAX hybrid monolith for hydrogen evolution reaction

Cong Cui[a,b], Renfei Cheng[a,b], Chao Zhang[a], Xiaohui Wang[a,*]

[a] Shenyang National Laboratory for Materials Science, Institute of Metal Research, Chinese Academy of Sciences, Shenyang 110016, China
[b] School of Materials Science and Engineering, University of Science and Technology of China, Shenyang 110016, China

ARTICLE INFO

Article history:
Received 6 July 2019
Received in revised form 2 August 2019
Accepted 15 August 2019
Available online 16 August 2019

Keywords:
Clean energy
Hydrogen evolution reaction
Pt catalyst
MXene
Porous MAX phase

ABSTRACT

Designing efficient electrocatalysts with low Pt loadings for hydrogen evolution reaction (HER) is urgently required for renewable and sustainable energy conversion. Here, we report a strategy that Pt nanoparticulates are spontaneously immobilized on porous MXene/MAX monolith as HER catalysts by utilizing the redox reaction between $Ti_3C_2T_x$ MXene and $[PtCl_4]^{2-}$ in H_2PtCl_6 aqueous solution. By taking advantage of homogeneously distributed Pt nanoparticulates on highly electrically conductive porous $Ti_3C_2T_x/Ti_3AlC_2$ monolith, the as-prepared electrocatalysts show high catalytic performance for hydrogen evolution. Specifically, the binder-free electrocatalysts have Pt loadings as low as 8.9 μg/cm^2, with low overpotential of 43 mV at a current density of 10 mA/cm^2 and low Tafel slope that three times lower than porous $Ti_3C_2T_x/Ti_3AlC_2$ without Pt loading. This strategy offers a new approach to constructing ultra-low Pt-loading HER catalysts on the basis of *in situ* redox reaction between noble metal ions and MXenes.

Hydrogen is one of the most important clean energy sources with high energy density of 120–140 MJ/kg [1,2]. Efficient and safe hydrogen production technology is the prerequisite for usage of hydrogen energy. Among the hydrogen production methods, electrocatalytic water splitting is regarded to be efficient and sustainable [3–5]. It proceeds by hydrogen evolution reaction (HER) *via* the reduction of protons or water [6,7]. Up to now, considerable endeavors have been devoted to developing many types of non-noble metal catalysts for HER, such as metal sulfides, metal carbides, metal phosphides, metal oxides or hydroxides to replace the noble metal Pt [7]. Unfortunately, none of them outperforms Pt with highly efficient, low overpotential and fast kinetics in HER. Considering the low abundance of Pt on the earth [8,9], reducing the nanostructures or even atomically distributed Pt centers supported on catalysts could significantly decrease Pt usages and maximize atom efficiency [10,11].

MXenes are a large family of two-dimensional materials that are synthesized by selectively etching off the "A" layers from the layered ternary carbides or carbonitrides known as MAX phases [12–14]. MAX phases have a general formula of $M_{n+1}AX_n$ (n = 1, 2, 3), where M represents a transition metal; A is usually an IIIA or IVA element; and X stands for C and/or N [15–17]. At the expense of the A removal in fluoride-containing acidic solution, the "MX" layers are left behind with surface functional groups [18], they are named as MXenes. Earlier studies have demonstrated that several types of MXenes themselves exhibit good catalytic activity for HER such as Ti_2CT_x [19] and Mo_2CT_x [20]. Moreover, extensive efforts have been devoted to the reduction of noble-metal ions using MXenes without external reducing agent [21]. The spontaneous redox reaction makes the noble metals firmly anchor on the surface of MXenes. These noble metals include but not limit to: Pt, Pd, Ag and Au. Noble metals/MXenes composites have shown high performance in some fields such as surface-enhanced Raman spectroscopy [21], catalysis [22–24], electrochemical energy storage [25,26], wastewater treatment [27,28] and sensing applications [29,30]. Especially, single platinum atoms can immobilize on $Mo_2TiC_2T_x$ MXene by electrode position technique and show excellent electrocatalytic activity for HER, which highlights a new approach for high efficiency utilizing Pt as catalyst [31].

In addition to the choice of catalyst, controlling the surface morphology and dispersion of the catalyst to expose active sites are equally important for enhancing HER performance. Notably, in the electrochemical test and practical applications, polymer binders like Nafion or polytetrafluoroethylene are usually used to immobilize the catalysts on the electrode surfaces in case of the destruction from hydrogen bubbles. Whereas, these polymer binders may block active sites, inhibit diffusion and increase the

* Corresponding author.
E-mail address: wang@imr.ac.cn (X. Wang).

https://doi.org/10.1016/j.cclet.2019.08.026

electron transfer resistance [32]. Thus, designing binder-free catalyst with homogeneous noble metal nanoparticulates distributed on the support is believed to be a hopeful strategy to obtain high performance catalyst for HER.

Herein, we report the fabrication of binder-free HER catalysts by using porous $Ti_3C_2T_x$ MXene/Ti_3AlC_2 hybrid monolith as catalyst support and Pt nanoparticulates as active sites. In the manner of spontaneous redox reaction between $Ti_3C_2T_x$ MXene and $[PtCl_6]^{2-}$ complex ions, the Pt nanoparticles anchored on the highly electrically hybrid support exhibit high catalytic performance with low overpotential and good stability even with very low Pt loadings. This preliminary study provides a new strategy for developing highly efficient HER catalysts.

Fig. 1 shows the schematic of Pt immobilized on porous MXene/MAX hybrid monolith for HER. The porous MXene/MAX hybrid monolith was prepared from a porous Ti_3AlC_2 matrix. To obtain the porous Ti_3AlC_2 matrix, a Ti_3AlC_2/MgO composite was firstly prepared by reactive hot pressing of the blended powders of Ti, Al, graphite and MgO at 1450 °C for 1 h. The as-prepared Ti_3AlC_2/MgO composite was then cut into pieces with the dimensions of 13 mm × 8.4 mm × 1 mm. Considering the good stability of MAX phases in hydrochloric acid solution [33], these pieces were subsequently immersed into 1 mol/L hydrochloric acid solution to eliminate MgO through forming water soluble $MgCl_2$, leaving porous Ti_3AlC_2 as the matrix. After that, the porous Ti_3AlC_2 cuboids were partially etched in 40% HF aqueous solution to generate a thin layer of $Ti_3C_2T_x$ MXene on the outmost surface of the Ti_3AlC_2 grains composing of the porous MAX monolith. Very importantly, the interesting structure, *i.e.*, $Ti_3C_2T_x$ MXene endogenously grown on the Ti_3AlC_2, enables the firm bonding between $Ti_3C_2T_x$ and Ti_3AlC_2 matrix and guarantees the good electronic conduction for HER. Finally, the porous $Ti_3C_2T_x$/Ti_3AlC_2 hybrid monolith was immersed into 1 mL of H_2PtCl_6 aqueous solution to trigger the spontaneous redox reaction between $Ti_3C_2T_x$ and $[PtCl_6]^{2-}$. As a result, Pt nanoparticulates were firmly anchored on the surface of $Ti_3C_2T_x$ MXene. Two concentrations of H_2PtCl_6 aqueous solutions were selected as 0.1 and 1 mmol/L to prepare two types of porous $Ti_3C_2T_x$/Ti_3AlC_2 monoliths with different Pt loadings, which are denoted as $Ti_3C_2T_x$@0.1 Pt and $Ti_3C_2T_x$@1 Pt, respectively. The corresponding Pt loadings do not exceed 8.9 μg/cm^2 or 88.9 μg/cm^2 for $Ti_3C_2T_x$@0.1 Pt and $Ti_3C_2T_x$@1 Pt, respectively. The optical photographs of the as-prepared samples are shown in Fig. S1 (Supporting information).

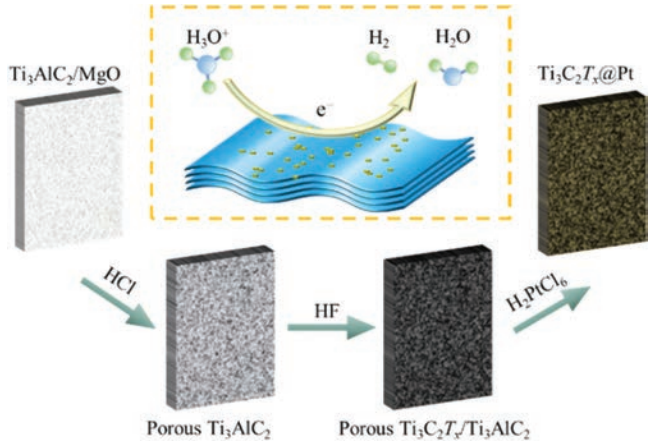

Fig. 1. Schematic of preparation of $Ti_3C_2T_x$@Pt catalysts. Firstly, Ti_3AlC_2/MgO pieces were immersed into hydrochloric acid solution to eliminate MgO, leaving porous Ti_3AlC_2 as the matrix. After that, the porous Ti_3AlC_2 were partially etched in 40% HF aqueous solution to generate $Ti_3C_2T_x$ MXene on the surface of porous Ti_3AlC_2. Finally, the porous $Ti_3C_2T_x$/Ti_3AlC_2 composites were immersed into H_2PtCl_6 aqueous solution to trigger the spontaneous redox reaction between $Ti_3C_2T_x$ and $[PtCl_6]^{2-}$.

As shown in Fig. S2 (Supporting information), the Ti_3AlC_2/MgO composite was prepared by using MgO as pore forming agent. To the best of our knowledge, the Ti_3AlC_2/MgO composite was reported in the literature for the first time. Considering the MgO is inert to many MAX phases, the method report in this work may be applicable to fabricate other MAX phases/MgO composite. With immersion in diluted hydrochloric acid solution, the MgO as pore forming agent was completely removed, giving rise to porous Ti_3AlC_2 monolith. Fig. S3 (Supporting information) exhibits the morphology and energy dispersive spectroscopy (EDS) elemental mapping of Ti_3AlC_2/MgO composite. As shown in Fig. S4 (Supporting information), after 1 mol/L hydrochloric acid solution treatment, almost all the MgO were eliminated, leaving the micron-sized holes on the surface of Ti_3AlC_2, which is well identified by EDS elemental mapping results and in consist with the XRD results (Fig. S2). The present method represents a facile approach to prepare porous MAX phases. As shown in Fig. S5 (Supporting information), the Raman spectra of Ti_3AlC_2/MgO composite and porous Ti_3AlC_2 are comparable in terms of well-recognized Raman bands assignable to Ti_3AlC_2 [34,35], which unambiguously indicates that the near surface of Ti_3AlC_2 grains are still highly lattice ordered and hydrochloric acid solution treatment do not introduce many defects on the surface of Ti_3AlC_2 grains. Due to the strong diffraction from Ti_3AlC_2 and much less contents of $Ti_3C_2T_x$ MXene and Pt, the diffraction peaks of $Ti_3C_2T_x$ MXene and Pt were hardly observed (Fig. S6 in Supporting information). In stark contrast, as a surface sensitive analysis method, Raman spectroscopy recognizes strong Raman peaks belonging to $Ti_3C_2T_x$ MXene [12,36,37], as shown in Fig. S7 (Supporting information). Upon loading Pt, the Raman bands of MXene for the $Ti_3C_2T_x$@0.1 Pt are observable, while they are invisible for the $Ti_3C_2T_x$@1 Pt.

To understand the spontaneous formation of Pt nanoparticulates on $Ti_3C_2T_x$ MXene, we comprehensively investigated the porous $Ti_3C_2T_x$/Ti_3AlC_2 hybrid monolith before and after H_2PtCl_6 aqueous solution treatment. Fig. 2 shows the XPS spectra for Ti 2p and Pt 4f of porous $Ti_3C_2T_x$/Ti_3AlC_2 and $Ti_3C_2T_x$@1 Pt. As shown in Fig. 2a, the functional groups of −O increased while −OH decreased after H_2PtCl_6 aqueous solution treatment, which proves the valence of Ti increased in MXene [36,38], as a result of electron donation from Ti. Correspondingly, the Pt 4f peaks corresponding to metallic Pt is well recognized for the sample after 1 mmol/L H_2PtCl_6 aqueous solution treatment. The formation of metallic Pt is believed to the reduction of Pt cations as the result of accepting electrons from $Ti_3C_2T_x$ MXene.

According to morphological analysis by scanning electron microscopy (SEM), the surface of as-etched porous Ti_3AlC_2 exhibits typical morphology of MXenes with aligned microslits (Figs. 3a and

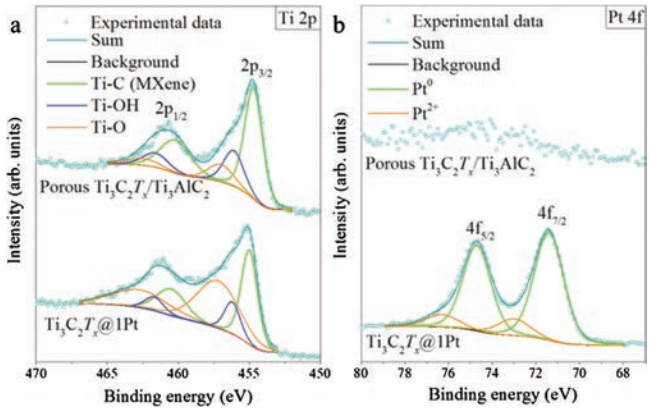

Fig. 2. XPS analysis of (a) Ti 2p in porous $Ti_3C_2T_x$/Ti_3AlC_2, $Ti_3C_2T_x$@1 Pt and (b) Pt 4f in porous $Ti_3C_2T_x$/Ti_3AlC_2, $Ti_3C_2T_x$@1 Pt.

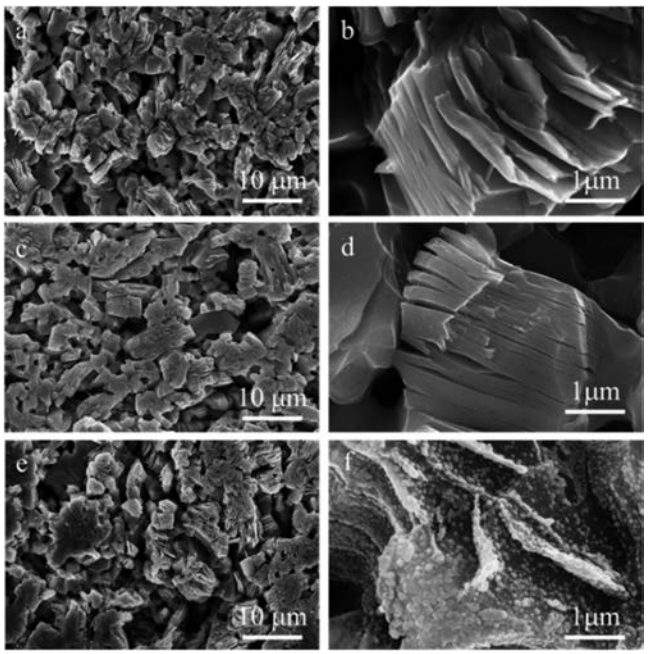

Fig. 3. Low magnification SEM images of (a) porous $Ti_3C_2T_x/Ti_3AlC_2$, (c) $Ti_3C_2T_x$@0.1 Pt, (e) $Ti_3C_2T_x$@1 Pt and high magnification SEM images of (b) porous $Ti_3C_2T_x/Ti_3AlC_2$, (d) $Ti_3C_2T_x$@0.1 Pt, (f) $Ti_3C_2T_x$@1 Pt.

b). With low Pt loadings, for $Ti_3C_2T_x$@0.1 Pt, it is morphologically hard to identify the presence of Pt on the surface of MXene within the resolution of SEM (Figs. 3c and d). With the assistance of transmission electron microscopy (TEM), the existence of Pt ultra-small nanoparticulates has been confirmed in Fig. S8 (Supporting information). In stark contrast, with high Pt loadings, for $Ti_3C_2T_x$@1 Pt, Pt nanoparticles are distributed on the surface of porous $Ti_3C_2T_x/Ti_3AlC_2$, which are morphologically observed by SEM (Figs. 3e and f).

The HER activities of the catalysts were evaluated in a three-electrode system containing 0.5 mol/L H_2SO_4 aqueous solution. Fig. 4a exhibits the polarization curves of porous Ti_3AlC_2, porous $Ti_3C_2T_x/Ti_3AlC_2$, $Ti_3C_2T_x$@0.1 Pt and $Ti_3C_2T_x$@1 Pt respectively. The potential to reach HER current density (j) of -10 mA/cm^2 is a key

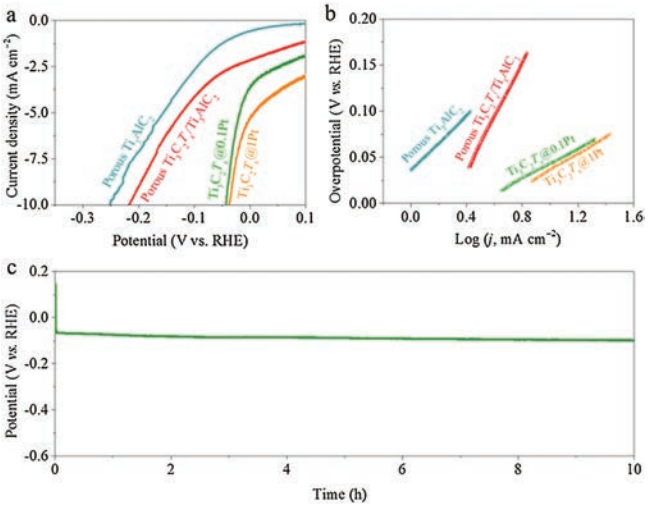

Fig. 4. Electrochemical HER performance characterizations. (a) HER polarization curves and (b) corresponding Tafel plots of porous Ti_3AlC_2, porous $Ti_3C_2T_x/Ti_3AlC_2$ and $Ti_3C_2T_x$@Pt; (c) Potential *vs.* time (V–t) curve of $Ti_3C_2T_x$@0.1 Pt recorded for 10 h at the current density of –10 mA/cm^2.

HER performance metric [10]. The porous Ti_3AlC_2 and porous $Ti_3C_2T_x$ request the overpotentials of -251 mV and -219 mV *vs.* reversible hydrogen electrode (RHE) for $j = -10$ mA/cm^2 electrode current respectively. In stark contrast, the overpotentials to reach -10 mA/cm^2 are 43 mV and 37 mV for $Ti_3C_2T_x$@0.1 Pt and $Ti_3C_2T_x$@1 Pt respectively. The close overpotentials indicate that MXene@Pt exhibit high catalytic activity even at very low platinum loadings, which is critical for future commercial applications. Higher Pt loadings show better performance on high current density (Fig. S9 in Supporting information). To gain insights on the HER kinetics for these catalysts, the Tafel slopes were calculated. As is presented in Fig. 4b, the Tafel slope of porous Ti_3AlC_2 is 148 mV per decade (mV/dec) while the porous $Ti_3C_2T_x/Ti_3AlC_2$ is 292 mV/dec. As high-performance pseudosupercapacitor material, $Ti_3C_2T_x$ MXene will generate capacitance before HER. In another word, the reaction between H^+ ions in H_2SO_4 aqueous solution and $-O$ functional groups of $Ti_3C_2T_x$ contributes the current before HER [36]. That is the reason why the Tafel slope of $Ti_3C_2T_x$ MXene is higher than porous Ti_3AlC_2 even though the porous $Ti_3C_2T_x/Ti_3AlC_2$ shows lower overpotential for HER at the same current density. Upon loading Pt on MXene, the Tafel slops of $Ti_3C_2T_x$@Pt decrease overtly and are 80 mV/dec and 89 mV/dec for $Ti_3C_2T_x$@0.1 Pt and $Ti_3C_2T_x$@1 Pt, respectively. The higher loading means that $[PtCl_6]^{2-}$ complex ions obtain more electrons from Ti in $Ti_3C_2T_x$ MXene and more $-OH$ functional groups convert to $-O$ functional groups. This makes $Ti_3C_2T_x$@1 Pt possesses higher current density than $Ti_3C_2T_x$@0.1 Ptbefore HER so that the Tafel slope of $Ti_3C_2T_x$@Pt increase when $Ti_3C_2T_x$ were loaded more Pt. Furthermore, electrochemical impedance spectroscopy (EIS) was performed to investigate the kinetics of the various samples. Fig. S10 (Supporting information) shows the spectra that collected at the potential of -5 mV *vs.* RHE. The $Ti_3C_2T_x$@0.1 Pt exhibits similar kinetics behavior to porous $Ti_3C_2T_x/Ti_3AlC_2$ because of the low Pt loadings. In stark contrast, $Ti_3C_2T_x$@1 Pt shows downward arc at low frequency region, which is related to HER. The difference in electrochemically active surface areas (ECSAs) of various samples was also evaluated *via* a simple cyclic voltammetry method. Interestingly, the $Ti_3C_2T_x$@0.1 Pt exhibits the highest value rather than $Ti_3C_2T_x$@1 Pt, which suggests that the HER is more dependent on the contents of Pt nanoparticulates than ECSAs (Fig. S11 in Supporting information). A long-term stability testing on $Ti_3C_2T_x$@0.1 Pt was also carried out by means of galvanostatic test. As is shown in Fig. 4c, $Ti_3C_2T_x$@0.1 Pt shows low voltage increasing over 10 h at a constant current density (10 mA/cm^2) operation.

In summary, we have fabricated Pt-immobilized partially etched MXene/MAX hybrid monolith as high-performance catalysts for HER through the spontaneous redox reaction between $[PtCl_6]^{2-}$ and MXene. This strategy takes the advantages of the good stability of MAX phases in acidic solution, high electronic conductivity and firm bonding between MXene and MAX phase. The catalyst shows low overpotential *vs.* RHE (43 mV for -10 mA/cm^2) based on low Pt loadings (lower than 8.9 μg/cm^2). This work not only provides the strategy to fabricate Pt-based catalyst for HER, but also paves avenues to further exploration and design of highly efficient catalysts based on noble metals and porous MXenes/MAX phases monoliths for other reactions.

Acknowledgments

This work was supported by the Youth Innovation Promotion Association, Chinese Academy of Sciences (CAS) (No. 2011152), Shenyang National Laboratory for Materials Science, Institute of Metal Research, CAS and by Special Program for Applied Research on Super Computation of the NSFC-Guangdong Joint Fund (the second phase) (No. U1501501).

Appendix A. Supplementary data

Supplementary material related to this article can be found, in the online version, at doi:https://doi.org/10.1016/j.cclet.2019.08.026.

References

[1] C.W. Hamilton, R.T. Baker, A. Staubitz, I. Manners, Chem. Soc. Rev. 38 (2009) 279–293.
[2] A. Midilli, M. Ay, I. Dincer, M.A. Rosen, Renew. Sust. Energ. Rev. 9 (2005) 255–271.
[3] T.E. Mallouk, Nat. Chem. 5 (2013) 362–363.
[4] P.P. Edwards, V.L. Kuznetsov, W.I.F. David, N.P. Brandon, Energ. Policy 36 (2008) 4356–4362.
[5] I. Dincer, C. Acar, Int. J. Hydrogen Energ. 40 (2015) 11094–11111.
[6] Y. Zheng, Y. Jiao, M. Jaroniec, S.Z. Qiao, Angew. Chem. Int. Ed. 54 (2015) 52–65.
[7] X. Zou, Y. Zhang, Chem. Soc. Rev. 44 (2015) 5148–5180.
[8] A.A. Yaroshevsky, Appl. Geochem. 44 (2006) 48–55.
[9] L. Tan, Y. Chi-Lung, Int. Geol. Rev. 12 (2009) 778–786.
[10] K. Jiang, B. Liu, M. Luo, et al., Nat. Commun. 10 (2019) 1743.
[11] Z. Zhang, Y. Chen, L. Zhou, et al., Nat. Commun. 10 (2019) 1657.
[12] M. Naguib, M. Kurtoglu, V. Presser, et al., Adv. Mater. 23 (2011) 4248–4253.
[13] M. Naguib, O. Mashtalir, J. Carle, et al., ACS Nano 6 (2012) 1322–1331.
[14] B. Anasori, M.R. Lukatskaya, Y. Gogotsi, Nat. Rev. Mater. 2 (2017) 16098.
[15] M.W. Barsoum, Prog. Solid State Ch 28 (2000) 201–281.
[16] Z.M. Sun, Int. Mater. Rev. 56 (2013) 143–166.
[17] X.H. Wang, Y.C. Zhou, J. Mater. Sci. Technol. 26 (2010) 385–416.
[18] T. Hu, Z. Li, M. Hu, et al., J. Phys. Chem. C 121 (2017) 19254–19261.
[19] S. Li, P. Tuo, J. Xie, et al., Nano Energy 47 (2018) 512–518.
[20] Z.W. Seh, K.D. Fredrickson, B. Anasori, et al., ACS Energy Lett. 1 (2016) 589–594.
[21] E. Satheeshkumar, T. Makaryan, A. Melikyan, et al., Sci. Rep. 6 (2016) 32049.
[22] K. Li, T. Jiao, R. Xing, et al., Sci. China Mater. 61 (2018) 728–736.
[23] Y.Y. Yuan, H.S. Li, L.G. Wang, et al., ACS Sustain. Chem. Eng. 7 (2019) 4266–4273.
[24] Z.W. Zhang, H.N. Li, G.D. Zou, et al., ACS Sustain. Chem. Eng. 4 (2016) 6763–6771.
[25] G. Zou, Z. Zhang, J. Guo, et al., ACS Appl. Mater. Inter. 8 (2016) 22280–22286.
[26] L. Li, N. Zhang, M.Y. Zhang, et al., ACS Sustain. Chem. Eng. 6 (2018) 7442–7450.
[27] X.X. Huang, R. Wang, T.F. Jiao, et al., ACS Omega 4 (2019) 1897–1906.
[28] R.P. Pandey, K. Rasool, V.E. Madhavan, et al., J. Mater. Chem. A: Mater. Energy Sustain. 6 (2018) 3522–3533.
[29] R.B. Rakhi, P. Nayak, C. Xia, H.N. Alshareef, Sci. Rep. 6 (2016) 36422.
[30] J.S. Zheng, B. Wang, A.L. Ding, et al., Electroanal. Chem. 816 (2018) 189–194.
[31] J. Zhang, Y. Zhao, X. Guo, et al., Nat. Catal. 1 (2018) 985–992.
[32] K. Xiong, L. Li, L. Zhang, et al., J. Mater. Chem. A: Mater. Energy Sustain. 3 (2015) 1863–1867.
[33] J. Xie, X. Wang, A. Li, F. Li, Y. Zhou, Corros. Sci. 60 (2012) 129–135.
[34] V. Presser, M. Naguib, L. Chaput, et al., J. Raman Spectrosc. 43 (2012) 168–172.
[35] H. Zhang, X.H. Wang, H.M. Xiang, Z.J. Li, Y.C. Zhou, Appl. Phys. Lett. 104 (2014) 131903.
[36] M. Hu, Z. Li, T. Hu, et al., ACS Nano 10 (2016) 11344–11350.
[37] T. Hu, J.M. Wang, H. Zhang, et al., Phys. Chem. Chem. Phys. 17 (2015) 9997–10003.
[38] M.R. Lukatskaya, S.M. Bak, X.Q. Yu, et al., Adv. Energy Mater. 5 (2015) 1500589.